

Application of equation-of-motion coupled-cluster methods to low-lying singlet and triplet electronic states of HBO and BOH

Nathan J. DeYonker,^{a)} Se Li, Yukio Yamaguchi, and Henry F. Schaefer III
Center for Computational Chemistry, University of Georgia, Athens, Georgia 30602

T. Daniel Crawford
Department of Chemistry, Virginia Tech, Blacksburg, Virginia 24061

Rollin A. King
Department of Chemistry, Bethel University, St. Paul, Minnesota 55112

Kirk A. Peterson
Department of Chemistry, Washington State University, Pullman, Washington 99164

(Received 24 March 2004; accepted 13 April 2005; published online 22 June 2005)

The equilibrium structures and physical properties of the $\tilde{X}^1\Sigma^+$ linear electronic states, linear excited singlet and triplet electronic states of hydroboron monoxide (HBO) ($\tilde{A}^1\Sigma^-$, $\tilde{B}^1\Delta$, $\tilde{a}^3\Sigma^+$, and $\tilde{b}^3\Delta$) and boron hydroxide (BOH) ($\tilde{A}^1\Sigma^+$, $\tilde{B}^1\Pi$, and $\tilde{b}^3\Pi$), and their bent counterparts (HBO \tilde{a}^3A' , \tilde{b}^3A' , \tilde{A}^1A' , \tilde{B}^1A' and BOH \tilde{X}^1A' , \tilde{b}^3A' , \tilde{c}^3A' , \tilde{A}^1A' , \tilde{B}^1A' , \tilde{C}^1A'') are investigated using excited electronic state *ab initio* equation-of-motion coupled-cluster (EOM-CC) methods. A new implementation of open-shell EOM-CC including iterative partial triple excitations (EOM-CC3) was tested. Coupled-cluster wave functions with single and double excitations (CCSD), single, double, and iterative partial triple excitations (CC3), and single, double, and full triple excitations (CCSDT) are employed with the correlation-consistent quadruple and quintuple zeta basis sets. The linear HBO $\tilde{X}^1\Sigma^+$ state is predicted to lie 48.3 kcal mol⁻¹ (2.09 eV) lower in energy than the BOH $\tilde{X}^1\Sigma^+$ linear stationary point at the CCSDT level of theory. The CCSDT BOH barrier to linearity is predicted to lie 3.7 kcal mol⁻¹ (0.16 eV). With a harmonic zero-point vibrational energy correction, the HBO $\tilde{X}^1\Sigma^+$ –BOH \tilde{X}^1A' energy difference is 45.2 kcal mol⁻¹ (1.96 eV). The lowest triplet excited electronic state of HBO, \tilde{a}^3A' , has a predicted excitation energy (T_e) of 115 kcal mol⁻¹ (4.97 eV) from the HBO ground state minimum, while the lowest-bound BOH excited electronic state, \tilde{b}^3A' , has a T_e of 70.2 kcal mol⁻¹ (3.04 eV) with respect to BOH \tilde{X}^1A' . The T_e values predicted for the lowest singlet excited states are $\tilde{A}^1A' \leftarrow \tilde{X}^1\Sigma^+ = 139$ kcal mol⁻¹ (6.01 eV) for HBO and $\tilde{A}^1A' \leftarrow \tilde{X}^1A' = 102$ kcal mol⁻¹ (4.42 eV) for BOH. Also for BOH, the triplet vertical transition energies are $\tilde{b}^3A' \leftarrow \tilde{X}^1A' = 71.4$ kcal mol⁻¹ (3.10 eV) and $\tilde{c}^3A' \leftarrow \tilde{X}^1A' = 87.2$ kcal mol⁻¹ (3.78 eV). © 2005 American Institute of Physics. [DOI: 10.1063/1.1927078]

I. INTRODUCTION

Hydroboron monoxide (HBO) is an intermediate or by-product of many reactions involving boron compounds.^{1–4} Boron-containing compounds are candidates for fuel additives^{5,6} and solid propellants that can increase rocket motor efficiency.^{7,8} HBO and its isomer boron hydroxide (BOH) have long been targets of experimental and theoretical studies. In the mid-1960s, HBO was first observed in the trimeric gas-phase form, boroxine (H₃B₃O₃), as a product of high-energy^{9,10} and combustion reactions.¹¹ Shortly thereafter, Lory and Porter identified monomeric HBO in an argon matrix and reported its vibrational frequencies.¹²

The first theoretical study on the HBO/BOH system was performed by Thomson and Wishart¹³ in 1974. It was concluded from a Mulliken population analysis¹⁴ that HBO has an unusual B–O bond order between two and three, demon-

strating an electron-deficient boron center. In 1977, Summers and Tyrrell¹⁵ reported a Hartree–Fock study of isoelectronic 14-electron species, determining the equilibrium geometry of linear BOH to have a higher energy than that of linear HBO. In 1979 Zyubina *et al.*¹⁶ were the first to analyze a potential-energy surface (PES) of the isomerization from HBO to BOH and noted some similarity to the PES for the isoelectronic linear HCN→HNC isomerization.¹⁷ Unlike HCN/HNC, when polarization functions were included in the basis set, a local minimum for bent BOH was discovered at $\angle\text{BOH} = 125^\circ$ lying 4.1 kcal mol⁻¹ lower in energy than that for linear BOH. As such, BOH is an unusual violator of the Walsh–Mulliken qualitative molecular orbital (MO) rules for 14-electron systems.^{18–23}

In 1986, the first gas-phase detection of monomeric HBO by Hirota's group using the discharge modulation technique renewed interest in the electronic structure of HBO.^{24–26} Infrared and microwave spectroscopy confirmed a

^{a)}Electronic mail: nate@ccqc.uga.edu

linear HBO structure and provided gas-phase vibrational frequencies and rotational spectra. These experimental studies were followed by theoretical papers analyzing linear and bent ground states using correlated methods such as Møller–Plesset perturbation theory,^{27–29} coupled-cluster,³⁰ and quadratic configuration interaction.^{31–33} These studies predicted the energy difference between the two isomers to be in a range of 44–51 kcal mol⁻¹ and a HBO→BOH isomerization reaction barrier-height range of 71–80 kcal mol⁻¹.

In 1995, Gole and Michels³¹ provided isomerization PESs for the ground states and lowest ³A' states of HBO and BOH using quadratic configuration interaction with single and double excitations and a perturbative triples correction [QCISD(T)]. They speculated that if crystalline BOH could be created, it might be able to release considerable energy upon controlled photochemical activation to excited electronic states and subsequent radiative relaxation to ground state HBO. At the ∠BOH angle of 53.0°, near where the first ³A' isomerization transition state (TS) is expected to be found, the ground state BOH PES is still fairly shallow. If this system is promoted from ground state BOH to a vibrationally excited level of the first ³A' state with a photon energy of ~3.7 eV, BOH may be able to undergo facile cyclic interconversion. If BOH is in fact a possible high-energy density material (HEDM),^{34–37} the hypothesis of Gole and Michels would be novel.

The 1999 study by Boldyrev and Simons³² focused on the HBO and BOH cations and reported not only that the $\tilde{X}^1\Sigma^+$ HBO→ $\tilde{X}^2\Pi$ HBO⁺ adiabatic ionization energy of 13.2 eV is far higher than that of BOH (9.6 eV), but also that BOH⁺ had a linear ground state ($\tilde{X}^2\Sigma^+$) rather different from $\tilde{X}^2\Pi$ HBO⁺. These differences originate from the large energy gap of the π -highest occupied molecular orbital (HOMO)/ π -lowest unoccupied molecular orbital (LUMO) of HBO versus the small σ -HOMO/ σ -LUMO energy gap of BOH.

A recent (2004) theoretical study conducted by Peng *et al.*³⁸ recognized the need to use multireference methods to appropriately ascertain the wave functions of HBO/BOH excited electronic states. Energy points on the isomerization PESs were obtained for the first two HBO/BOH triplet states using second-order multireference Brillouin–Wigner perturbation theory (MRBWPT2) and the correlation-consistent polarized valence triple zeta (cc-pVTZ) basis sets. Peng *et al.* reported a ground-state isomer energy difference (54.4 kcal mol⁻¹) that was 4 kcal mol⁻¹ higher than those of previous coupled-cluster studies.³⁰

Though the singlet-triplet excitations investigated in Refs. 31 and 38 are of a spin-forbidden nature, if enough intensity borrowing is available from nearby singlet excited states, the singlet-triplet electronic transition would possess an appreciable oscillator strength³⁹ and the mechanism proposed by Gole and Michels could be possible. While a singlet-singlet BOH electronic transition would have a large oscillator strength, its lifetime would be orders of magnitude shorter than that of a singlet-triplet transition. In this situation, the BOH molecule would likely fluoresce back to its ground state before isomerization towards a strongly exo-

thermic reaction pathway could occur. Although Gole and Michels have outlined explicit recipes for synthesizing and characterizing BOH,³¹ that research has not yet been experimentally realized.

To our knowledge, there are no published reports detailing the isomerization PESs of the HBO and BOH singlet excited electronic states. A more accurate theoretical prediction of excitation energies would validate the possibility of intensity borrowing between the BOH $\tilde{A}^1A'/^3A'$ states for the proposed HEDM pathway. Our task in this research is to examine some low-lying singlet and triplet excited states of HBO and BOH using excited state coupled-cluster techniques.

II. ELECTRONIC STRUCTURE CONSIDERATIONS

The electronic configuration of $\tilde{X}^1\Sigma^+$ HBO is qualitatively described as

$$[\text{core}]3\sigma^24\sigma^25\sigma^21\pi^4, \quad \tilde{X}^1\Sigma^+, \text{HBO}.$$

The symbol [core] pertains to the occupied 1s-like oxygen and boron orbitals. The ground electronic configuration of the linear BOH molecule is expressed, noting that the 1 π orbital is lower in energy than the 5 σ orbital,

$$[\text{core}]3\sigma^24\sigma^21\pi^45\sigma^2, \quad \tilde{X}^1\Sigma^+, \text{BOH}.$$

For the bent ground state of BOH, the occupied 1 π orbital of linear BOH splits into the 5a' and 1a'' MOs.⁴⁰ The 5a' orbital is more stabilized than the 1a'' orbital, a result opposite to the prediction from Walsh diagrams.¹⁸ The bent electronic configuration is expressed as

$$[\text{core}](3a')^2(4a')^2(5a')^2(1a'')^2(6a')^2, \quad \tilde{X}^1A'.$$

For linear HBO and BOH, the manifold of singly excited electronic states arises from the following types of electronic excitation:

- (a) Promotion of a 1 π electron to one of the antibonding 2 π orbitals. Six excited electronic states can be derived from this single excitation,

$$[\text{core}]3\sigma^24\sigma^25\sigma^21\pi^32\pi, \quad ^1\Delta, ^1\Sigma^-, ^1\Sigma^+, ^3\Delta, ^3\Sigma^-, ^3\Sigma^+.$$

- (b) Promotion of a 5 σ electron to one of the antibonding 2 π orbitals. Two excited electronic states can be derived from this excitation,

$$[\text{core}]3\sigma^24\sigma^25\sigma^1\pi^42\pi, \quad ^1\Pi, ^3\Pi.$$

- (c) Promotion of a 1 π electron to the 6 σ antibonding MO, whereupon there are two excited electronic states,

$$[\text{core}]3\sigma^24\sigma^25\sigma^21\pi^36\sigma, \quad ^1\Pi, ^3\Pi.$$

- (d) Promotion of a 5 σ electron to the 6 σ MO, with the following two excited electronic states:

$$[\text{core}]3\sigma^24\sigma^25\sigma^1\pi^46\sigma, \quad ^1\Sigma^+, ^3\Sigma^+.$$

Thus, there are thirteen unique linear electronic states relevant to this study, including the ground electronic state.

The electronic configuration for the ${}^1\Delta$ state from $1\pi \rightarrow 2\pi$ excitation in real MO notation requires four Slater determinants. In C_{2v} point-group symmetry notation, where the linear molecule is in the Cartesian z axis, its A_1 and A_2 components are, in the simplest picture,

$$\begin{aligned} &[\text{core}]3\sigma^24\sigma^25\sigma^2 \times [(1\pi_x\alpha(1))(2\pi_x\beta(2))1\pi_y^2 \\ &\quad - (1\pi_x\beta(1))(2\pi_x\alpha(2))1\pi_y^2 \\ &\quad - (1\pi_y\alpha(1))(2\pi_y\beta(2))1\pi_x^2 \\ &\quad + (1\pi_y\beta(1))(2\pi_y\alpha(2))1\pi_x^2], \quad {}^1\Delta({}^1A_1), \end{aligned}$$

and

$$\begin{aligned} &[\text{core}]3\sigma^24\sigma^25\sigma^2 \times [(1\pi_x\alpha(1))(2\pi_y\beta(2))1\pi_y^2 \\ &\quad - (1\pi_x\beta(1))(2\pi_y\alpha(2))1\pi_y^2 \\ &\quad + (1\pi_y\alpha(1))(2\pi_x\beta(2))1\pi_x^2 \\ &\quad - (1\pi_y\beta(1))(2\pi_x\alpha(2))1\pi_x^2], \quad {}^1\Delta({}^1A_2). \end{aligned}$$

The ${}^1\Sigma^-$ excited state requires four Slater determinants for a proper description and is written in terms of real orbitals as

$$\begin{aligned} &[\text{core}]3\sigma^24\sigma^25\sigma^2 \times [(1\pi_x\alpha(1))(2\pi_y\beta(2))1\pi_y^2 \\ &\quad - (1\pi_x\beta(1))(2\pi_y\alpha(2))1\pi_y^2 - (1\pi_y\alpha(1)) \\ &\quad \times (2\pi_x\beta(2))1\pi_x^2 \\ &\quad + (1\pi_y\beta(1))(2\pi_x\alpha(2))1\pi_x^2], \quad {}^1\Sigma^-({}^1A_2). \end{aligned}$$

The open-shell ${}^1\Sigma^+$ wave function derived from the $1\pi \rightarrow 2\pi$ excitation is qualitatively described as

$$\begin{aligned} &[\text{core}]3\sigma^24\sigma^25\sigma^2 \times [(1\pi_x\alpha(1))(2\pi_x\beta(2))1\pi_y^2 \\ &\quad - (1\pi_x\beta(1))(2\pi_x\alpha(2))1\pi_y^2 \\ &\quad + (1\pi_y\alpha(1))(2\pi_y\beta(2))1\pi_x^2 \\ &\quad - (1\pi_y\beta(1))(2\pi_y\alpha(2))1\pi_x^2], \quad {}^1\Sigma^+({}^1A_1). \end{aligned}$$

The two degenerate components of the ${}^3\Delta$ state are written as

$$\begin{aligned} &[\text{core}]3\sigma^24\sigma^25\sigma^2 \times [(1\pi_x\alpha(1))(2\pi_x\alpha(2))1\pi_y^2 \\ &\quad - (1\pi_y\alpha(1))(2\pi_y\alpha(2))1\pi_x^2], \quad {}^3\Delta({}^3A_1) \end{aligned}$$

and

$$\begin{aligned} &[\text{core}]3\sigma^24\sigma^25\sigma^2 \times [(1\pi_x\alpha(1))(2\pi_y\alpha(2))1\pi_y^2 \\ &\quad + (1\pi_y\alpha(1))(2\pi_x\alpha(2))1\pi_x^2], \quad {}^3\Delta({}^3A_2). \end{aligned}$$

The ${}^3\Sigma^-$ wave function is

$$\begin{aligned} &[\text{core}]3\sigma^24\sigma^25\sigma^2 \times [(1\pi_x\alpha(1))(2\pi_y\alpha(2))1\pi_y^2 \\ &\quad - (1\pi_y\alpha(1))(2\pi_x\alpha(2))1\pi_x^2], \quad {}^3\Sigma^-({}^3A_2). \end{aligned}$$

Lastly, the ${}^3\Sigma^+$ wave function from $1\pi \rightarrow 2\pi$ single excitations is

$$\begin{aligned} &[\text{core}]3\sigma^24\sigma^25\sigma^2 \times [(1\pi_x\alpha(1))(2\pi_x\alpha(2))1\pi_y^2 \\ &\quad + (1\pi_y\alpha(1))(2\pi_y\alpha(2))1\pi_x^2], \quad {}^3\Sigma^+({}^3A_1). \end{aligned}$$

From the $5\sigma \rightarrow 2\pi$ single excitation, the 1B_1 component of the following ${}^1\Pi$ electronic state wave function can be described as

TABLE I. Valence molecular orbital (MO) ordering of HBO and BOH in C_{2v} and C_s point group symmetries. Note that in-plane bending is considered to occur in the yz plane. MO energy increases downwards.

HBO C_{2v}	HBO C_s	BOH C_{2v}	BOH C_s
3σ	$3a'$	3σ	$3a'$
4σ	$4a'$	4σ	$4a'$
5σ	$5a'$	$1\pi_x$	$1a''$
$1\pi_x$ (HOMO)	$1a''$ (HOMO)	$1\pi_y$	$5a'$
$1\pi_y$ (HOMO)	$6a'$ (HOMO)	5σ (HOMO)	$6a'$ (HOMO)
$2\pi_x$ (LUMO)	$2a''$ (LUMO)	6σ (LUMO)	$7a'$ (LUMO)
$2\pi_y$ (LUMO)	$7a'$ (LUMO)	$2\pi_x$	$2a''$
6σ	$8a'$	$2\pi_y$	$8a'$

$$\begin{aligned} &[\text{core}]3\sigma^24\sigma^21\pi^4 \times [(5\sigma\alpha(1))(2\pi_x\beta(2)) \\ &\quad - (5\sigma\beta(1))(2\pi_x\alpha(2))], \quad {}^1\Pi({}^1B_1), \end{aligned}$$

and its triplet 3B_1 counterpart is

$$[\text{core}]3\sigma^24\sigma^21\pi^4(5\sigma\alpha(1))(2\pi_x\alpha(2)), \quad {}^3\Pi({}^3B_1).$$

Arising from the $1\pi \rightarrow 6\sigma$ single excitation, the 1B_1 component of the ${}^1\Pi$ electronic state wave function can be described as

$$\begin{aligned} &[\text{core}]3\sigma^24\sigma^25\sigma^2 \times [(1\pi_x\alpha(1))(6\sigma\beta(2))1\pi_y^2 \\ &\quad - (1\pi_x\beta(1))(6\sigma\alpha(2))1\pi_y^2], \quad {}^1\Pi({}^1B_1), \end{aligned}$$

with the corresponding triplet 3B_1 wave function,

$$[\text{core}]3\sigma^24\sigma^25\sigma^2(1\pi_x\alpha(1))1\pi_y^2(6\sigma\alpha(2)), \quad {}^3\Pi({}^3B_1).$$

Finally, the wave functions of the two excited states owing to the $5\sigma \rightarrow 6\sigma$ single excitation are written as

$$\begin{aligned} &[\text{core}]3\sigma^24\sigma^21\pi^4 \times [(5\sigma\alpha(1))(6\sigma\beta(2)) \\ &\quad - (5\sigma\beta(1))(6\sigma\alpha(2))], \quad {}^1\Sigma^+({}^1A_1) \end{aligned}$$

and

$$[\text{core}]3\sigma^24\sigma^21\pi^4(5\sigma\alpha(1))(6\sigma\alpha(2)), \quad {}^3\Sigma^+({}^3A_1).$$

When the HBO and BOH linear isomers are bent, differences in their electronic structure create separate correspondence between their MOs of C_{2v} and C_s point-group symmetry. Translation of the $C_{\infty v}/C_{2v}$ MOs of HBO and BOH into C_s symmetry is shown in Table I and the wave functions of possible bent singly excited electronic states are listed in Supplementary Table S1.⁴¹

III. THEORETICAL METHODS

For single-reference methods, the zeroth-order description of $\tilde{X}{}^1\Sigma^+$ HBO and $\tilde{X}{}^1\Sigma^+$ BOH was obtained using restricted Hartree–Fock (RHF) wave functions. The zeroth-order descriptions of triplet states for coupled-cluster references were obtained with unrestricted HF (UHF) wave functions. Ground state dynamical correlation was accounted for using coupled-cluster methods^{42,43} with single and double excitations (CCSD),⁴⁴ single, double, and perturbative partial triple excitations [CCSD(T)],^{45,46} single, double, and iterative partial triple excitations (CC3),⁴⁷ and full triple excitations (CCSDT).^{48,49} For the excited electronic states, we

have made use of the equation-of-motion CCSD (EOM-CCSD)^{50,51} method as well as the CC3 model, which includes connected triple excitations. Although CC3 excitation energies are usually viewed from a linear-response perspective,⁵² we will use the EOM designation for both CCSD and CC3 excited states for the sake of simplicity.

The correlation-consistent polarized valence quadruple zeta (cc-pVQZ) basis sets developed by Dunning and co-workers were used in this study.^{53,54} Unless otherwise noted, in all correlated procedures the core $1s$ -like orbitals of oxygen and boron were frozen. Closed-shell and excited singlet state CC/EOM-CC computations were carried out using ACES II.⁵⁵ The open-shell triplet CC3, EOM-CCSD, and EOM-CC3 methods were employed in conjunction with the PSI 3.2 package.⁵⁶ The open-shell implementation of the CC3 and EOM-CC3 methods incorporated in PSI 3.2 were recently described in Ref. 56.

Structural optimizations and vibrational analyses were carried out at each level of theory using finite differences of energies. For $\tilde{X}^1\Sigma^+$ HBO and \tilde{X}^1A' BOH, fundamental vibrational frequencies were also determined at the CCSD(T) level of theory (with all electrons correlated due to program requirements) using second-order vibrational perturbation theory with cubic and semidiagonal quartic force constants computed via finite differences of analytic second derivatives using the method described by Stanton *et al.*⁵⁷

Explicitly for linear HBO, the stationary points of the following electronic states were investigated: the $\tilde{X}^1\Sigma^+$ ground state, the $\tilde{A}^1\Sigma^-$ state, the 1A_1 component of $\tilde{B}^1\Delta$, the $\tilde{a}^3\Sigma^+$ state, and the 3A_2 component of $\tilde{b}^3\Delta$, which all arise from the $1\pi \rightarrow 2\pi$ excitation. For BOH, the electronic states included were the $\tilde{X}^1\Sigma^+$ ground state, the $\tilde{a}^3\Sigma^+$ and $\tilde{A}^1\Sigma^+$ states from the $5\sigma \rightarrow 6\sigma$ excitation, and the $\tilde{b}^3\Pi$ and $\tilde{B}^1\Pi$ states from the $5\sigma \rightarrow 2\pi$ excitation. Tables I and S1 describe the wave functions for the bent counterparts of electronic states under investigation, and the state ordering of the bent states will be discussed below. The minima of the highest-lying HBO and BOH excited states characterized are 5.8 and 3.2 eV below the ionization potential,³² respectively. It is not likely that Rydberg excited states exist within these manifolds of electronic states.

IV. RESULTS AND DISCUSSION

A. Linear ground state of HBO

The total energies, equilibrium geometries, and physical properties of the linear singlet ground electronic states of HBO and BOH are reported in Table II. The equilibrium bond lengths of $\tilde{X}^1\Sigma^+$ HBO have been experimentally determined by gas-phase microwave spectroscopy to be $r_e(\text{HB}) = 1.1667 \pm 0.0004 \text{ \AA}$ and $r_e(\text{BO}) = 1.2007 \pm 0.0001 \text{ \AA}$.^{25,26} Coupled-cluster methods including triple excitations [CC3, CCSD(T), and CCSDT] reproduce the equilibrium geometry. The CCSD(T) $r_e(\text{BO})$ of 1.2019 \AA is only 0.0012 \AA longer than the derived gas phase $r_e(\text{BO})$. With the boron and oxygen $1s$ electrons correlated, the CCSD(T) geometries may represent a Pauling point for this electronic state. However, the frozen-core CC3 and CCSDT methods perform admirably,

and we prefer levels of theory with the core electrons frozen for the study of excited electronic states.

The CCSDT dipole moment of linear HBO has a magnitude of 2.70 D, with direction $^+\text{HBO}^-$. The large dipole moment implies a highly polar molecule. The harmonic $\omega_1(\sigma)$ BH stretching frequencies obtained using the CCSD(T), CC3, and CCSDT methods are 2899, 2885, and 2890 cm^{-1} , respectively. In the analysis performed by Kawashima *et al.*,²⁶ the observed fundamental $\nu_2(\pi)$ and $\nu_3(\sigma)$ frequencies were used as harmonic frequencies in order to estimate the harmonic $\omega_1(\sigma)$ BH stretching frequency, which may explain their rather low $\omega_1(\sigma)$ value of 2821 cm^{-1} . Using the all-electron CCSD(T) anharmonic correction, the fundamental $\nu_1(\sigma)$ frequency is shifted to 2810 cm^{-1} , in fair agreement with the more reasonable estimated value of $2849 \pm 10 \text{ cm}^{-1}$ given by Lory and Porter¹² in their IR matrix-isolation experiments. The CCSD(T) fundamental $\nu_2(\pi)$ bending frequency of 759 cm^{-1} and the $\nu_3(\sigma)$ BO stretching frequency of 1831 cm^{-1} (computed with all electrons correlated, as noted above) are correct to within 5 cm^{-1} of the respective gas-phase fundamental frequencies. However, the inclusion of anharmonicity is seen to raise the $\nu_2(\pi)$ bending frequency, a highly unusual effect.

Relative to the full CCSDT result, the triples contribution of the CC3 method to the $\tilde{X}^1\Sigma^+$ HBO and $\tilde{X}^1\Sigma^+$ BOH total energies are overestimated by $\sim 1 \text{ kcal mol}^{-1}$. However, CC3 geometries compare very favorably with the experimental and full CCSDT bond lengths, particularly in light of the computational savings offered.⁵⁸

B. Linear ground state of BOH

Table II shows energetic and geometric data for linear $\tilde{X}^1\Sigma^+$ BOH. The CCSDT geometry of $\tilde{X}^1\Sigma^+$ BOH is $r_e(\text{BO}) = 1.2791 \text{ \AA}$ and $r_e(\text{OH}) = 0.9493 \text{ \AA}$. The BO distance of $\tilde{X}^1\Sigma^+$ BOH is longer than that of $\tilde{X}^1\Sigma^+$ HBO because of a lessening of π overlap, and hence a weakening of the multiple bond character. This rather long BO bond is also an indicator of the preference towards a bent BOH minimum.

The CCSDT dipole moment of $\tilde{X}^1\Sigma^+$ BOH is larger than that of $\tilde{X}^1\Sigma^+$ HBO and of the opposite sign $^-\text{BOH}^+$, with a magnitude of 3.69 D. The OH $\omega_1(\sigma)$ stretching frequency from the CC3 and CCSDT methods is 4009 and 4018 cm^{-1} , respectively, and the BO stretching frequency $\omega_3(\sigma)$ is 1464 and 1473 cm^{-1} , respectively. Due to the elongated BO bond length, the $\omega_3(\sigma)$ frequency of $\tilde{X}^1\Sigma^+$ BOH is lower by approximately 360 cm^{-1} than the BO stretch of HBO. The bending frequency of $\tilde{X}^1\Sigma^+$ BOH is imaginary, signifying a bent equilibrium geometry for BOH. The imaginary CC3 and CCSDT $\omega_2(\pi)$ harmonic frequencies are $485i$ and $487i \text{ cm}^{-1}$.

The overestimation of the triple excitation contribution to the total energy using the CC3 method is largely canceled when considering relative energies. With all electrons correlated, the CCSD(T) energy separation between the linear ground states is predicted to be 49.2 kcal mol^{-1} . There is little effect due to core correlation on the harmonic zero-point vibrational energy (ZPVE), and the ZPVE-corrected energy difference between the HBO and BOH linear ground

TABLE II. Total energies and physical properties for the linear HBO and BOH ground electronic states. (Energies are in hartrees, bond distances in angstrom, dipole moments in debye, and harmonic vibrational frequencies in cm^{-1} .)

Level of theory	Energy	$r_e(\text{H}-\text{B})$	$r_e(\text{B}-\text{O})$	μ_e^a	$\omega_1(\sigma)$	$\omega_2(\pi)$	$\omega_3(\sigma)$
$\tilde{X}^1\Sigma^+$ HBO							
cc-pVQZ RHF	-100.212875	1.1643	1.1788	3.210	2994	863	2009
cc-pVQZ CCSD	-100.567370	1.1680	1.1983	2.799	2905	778	1882
cc-pVQZ CC3	-100.585344	1.1692	1.2075		2885	753	1810
cc-pVQZ CCSDT	-100.583483	1.1690	1.2048	2.703	2890	759	1838
cc-pVQZ CCSD(T) ^b	-100.641033	1.1663	1.2019	2.690	$\left\{ \begin{array}{l} \omega=2899 \\ \nu=2810 \end{array} \right.$	$\left\{ \begin{array}{l} \omega=749 \\ \nu=759 \end{array} \right.$	$\left\{ \begin{array}{l} \omega=1847 \\ \nu=1831 \end{array} \right.$
6-311++G(2df,2pd) ^c		1.169	1.208		2894	780	1825
cc-pVTZ MR-BWPT2 ^d		1.1590	1.2093				
TZ2P(f,d) CCSD(T) ^e		1.1694	1.2064	2.692	2888	766	1831
Experiment ^f		1.1667	1.2007		2821 ^g	$\nu=754$	$\nu=1826$
Experiment ^h					$\nu=2849$		
	Energy	$r_e(\text{B}-\text{O})$	$r_e(\text{O}-\text{H})$	μ_e^a	$\omega_1(\sigma)$	$\omega_2(\pi)$	$\omega_3(\sigma)$
$\tilde{X}^1\Sigma^+$ BOH							
cc-pVQZ RHF	-100.143860	1.2598	0.9319	3.872	4301	529i	1572
cc-pVQZ CCSD	-100.492240	1.2751	0.9462	3.687	4070	497i	1493
cc-pVQZ CC3	-100.507434	1.2804	0.9498		4009	485i	1464
cc-pVQZ CCSDT	-100.506530	1.2791	0.9493	3.687	4018	487i	1473
cc-pVQZ CCSD(T)	-100.562678	1.2748	0.9480	3.723	4027	472i	1486
6-311++G(2df,2pd) ^c		1.309	0.9630				
cc-pVTZ MR-BWPT2 ^d		1.2680	0.9493				
TZ2P(f,d) CCSD(T) ^e		1.2814	0.9508	3.660			

^aThe directions of the dipole moments are $^+\text{HBO}^-$ and $^-\text{BOH}^+$, respectively.

^bThe second set of CCSD(T) vibrational frequencies are fundamental frequencies computed via finite differences of analytic second derivatives. Due to program requirements in the analytic gradient code, all electrons were correlated when obtaining CCSD(T) data.

^cReference 32.

^dReference 38.

^eReference 30.

^fReference 24 and 26.

^gFrom Ref. 26, $\nu_2(\pi)$ and $\nu_3(\sigma)$ are observed fundamental frequencies, while the $\omega_1(\sigma)$ is an estimated harmonic frequency.

^hReference 12 is an Ar-matrix isolation experiment, and the fundamental frequency is estimated to have error bars of 10 cm^{-1} .

states is predicted to be $48.9 \text{ kcal mol}^{-1}$ with CC3 and $48.3 \text{ kcal mol}^{-1}$ with CCSDT. The extension of the basis set to correlation-consistent polarized valence quintuple zeta (cc-pV5Z) (at the CC3 cc-pVQZ geometries) increases the separation by just $0.1 \text{ kcal mol}^{-1}$. We are confident that the true energy difference between the linear isomers is near $48\text{--}49 \text{ kcal mol}^{-1}$.

C. Bent BOH ground state

The bent \tilde{X}^1A' BOH equilibrium geometry of the ground state in Table III has been discussed in a number of theoretical papers.^{30,31,38,40} The CCSDT bond lengths for the bent BOH \tilde{X}^1A' state increase (compared to the linear structure) due to destabilization of the π bonding. The CCSDT $r_e(\text{BO})$ prediction is 1.3051 \AA , $r_e(\text{OH})$ is 0.9617 \AA , and the BOH angle is 121.4° . Harmonic vibrational frequencies are similar to the BOH linear structure and the stretching frequencies are predicted to be $\omega_1(a')=3855 \text{ cm}^{-1}$ and $\omega_2(a')=1402 \text{ cm}^{-1}$, while the $\omega_3(a')$ BOH angle bend is predicted to be 619 cm^{-1} . The theoretical rovibrational study of HBO/BOH performed by Ha and Makarewicz²⁹ in 1999 sampled the PES of the \tilde{X}^1A' BOH state and presented evidence that the harmonic approximation will fail due to large

amplitude motion of the hydrogen nucleus around the BO bond. Indeed, the anharmonic corrections to the vibrational frequencies shift the values of the O–H stretching and BOH-angle bending significantly, as the all-electron CCSD(T) level of theory predicts the fundamental $\nu_1(a')$ to be 3679 cm^{-1} , $\nu_2(a')$ to be 1399 cm^{-1} , and the bending $\nu_3(a')$ to be 563 cm^{-1} . The CCSD(T) $\nu_2(a')$ and $\nu_3(a')$ fundamental vibrational frequencies obtained in our study are larger than the MP2 fundamental vibrational frequencies of Ha and Makarewicz²⁹ by 37 and 57 cm^{-1} , respectively. Hopefully the rovibrational parameters fit by Ha and Makarewicz and our improved fundamental vibrational frequencies will assist in the spectroscopic identification of the BOH ground state.

At the CCSDT level of theory, the \tilde{X}^1A' BOH minimum is predicted to be lower in energy than the linear stationary point by $3.7 \text{ kcal mol}^{-1}$. With the harmonic ZPVE correction, the energy difference between the $\tilde{X}^1\Sigma^+$ HBO and \tilde{X}^1A' BOH ground states is $45.2 \text{ kcal mol}^{-1}$. The CCSDT and CC3 methods are again in good agreement for the geometry and energetics, whereas the differences in quantities between CCSDT and CCSD shown in Table III are somewhat larger. It seems evident that the CC3 method is more reliable than

TABLE III. Total energies and geometric parameters of bent \tilde{X}^1A' BOH. (Energies are in hartrees, bond distances in angstrom, harmonic vibrational frequencies in cm^{-1} , and energy differences in kcal mol^{-1} .)

BOH \tilde{X}^1A'	Energy	$r_e(\text{B-O})$	$r_e(\text{O-H})$	$\angle\text{BOH}$	$\omega_1(a')$	$\omega_2(a')$	$\omega_3(a')$	ΔE^a
cc-pVQZ RHF	-100.150111	1.2854	0.9436	123.51	4127	1501	683	-3.92
cc-pVQZ CCSD	-100.498312	1.3018	0.9587	121.42	3901	1417	636	-3.81
cc-pVQZ CC3	-100.513218	1.3061	0.9621	121.45	3849	1396	615	-3.63
cc-pVQZ CCSDT	-100.512394	1.3051	0.9617	121.36	3855	1402	619	-3.68
cc-pVQZ CCSD(T) ^b	-100.568182	1.3003	0.9601	121.84	$\left\{ \begin{array}{l} \omega=3864 \\ \nu=3679 \end{array} \right.$	$\left\{ \begin{array}{l} \omega=1418 \\ \nu=1399 \end{array} \right.$	$\left\{ \begin{array}{l} \omega=613 \\ \nu=563 \end{array} \right.$	
TZ2P[<i>f, d</i>] CCSD(T) ^c		1.3068	0.9635	121.45	3852	1397	607	-3.51
6-311+G(2 <i>df, 2pd</i>) QCISD(T) ^d		1.309	0.963	121.1	3870	1393	616	
cc-pVTZ MR-BWPT2 ^d		1.2946	0.9597	123.96				-0.99
aug-cc-pVTZ MP2 ^f		1.298	0.962	124.2	$\nu=3680$	1436	$\nu=506$	-3.0

^aEnergy differences are relative to the optimized linear structure of $\tilde{X}^1\Sigma^+$ BOH.

^bThe second set of CCSD(T) vibrational frequencies are fundamental frequencies computed via finite differences of analytic second derivatives. Due to program requirements in the analytic gradient code, all electrons were correlated when obtaining CCSD(T) data.

^cReference 30.

^dReference 32.

^eReference 38.

^fReference 29.

CCSD for the HBO/BOH system, and it is expected that such accuracy can be translated to the EOM-CC3 predictions for the excited electronic states.

D. Linear HBO singlet excited states

The total energies and physical properties of the linear excited states are presented in Table IV. The two lowest-lying linear singlet excited states of HBO are the $\tilde{A}^1\Sigma^-$ and $\tilde{B}^1\Delta$ states, formed from $1\pi \rightarrow 2\pi$ excitation. As the two states possess the same dominant electronic configuration with different configuration state functions, their relative energies and geometries are similar. For both states, the $1\pi \rightarrow 2\pi$ excitation greatly increases the B-O bond distance

relative to the ground state. At the EOM-CC3 level, the $\tilde{A}^1\Sigma^-$ B-O bond distance is predicted to be 1.4219 Å, and that of the $\tilde{B}^1\Delta$ state $r_e(\text{BO})$ to be 1.4276 Å, implying a weak BO bond for both states. Higher in energy, the $\tilde{B}^1\Delta$ state has the weaker and slightly longer BO bond. Since electrons involved in the $\pi \rightarrow \pi^*$ excitation of these two states are localized on the boron and oxygen atoms, the EOM-CC3 HB bond distances of the first two singlet excited states remain within 0.003 Å of the $\tilde{X}^1\Sigma^+$ HBO value of $r_e(\text{HB})$. Compared to the EOM-CC3 bond length, the EOM-CCSD method provides a reasonable $r_e(\text{HB})$ for the HBO singlet excited states, but underestimates $r_e(\text{BO})$ by nearly 0.03 Å.

TABLE IV. Total energies and physical properties for linear HBO excited electronic states. [Energies are in hartrees, bond distances in angstrom, dipole moments in debye, harmonic vibrational frequencies in cm^{-1} , and transition energies in kcal mol^{-1} (eV, in parentheses) relative to the $\tilde{X}^1\Sigma^+$ HBO minimum.]

Level of theory	Energy	$r_e(\text{H-B})$	$r_e(\text{B-O})$	μ_e	$\omega_1(\sigma)$	$\omega_2(\pi)$	$\omega_3(\sigma)$	ΔE
HBO $\tilde{A}^1\Sigma^-$								
cc-pVQZ EOM-CCSD	-100.302082	1.1623	1.3945	0.842	2916	938 <i>i</i>	1222	166.5(7.22)
cc-pVQZ EOM-CC3	-100.326390	1.1655	1.4219		2882	974 <i>i</i>	1095	162.5(7.05)
HBO $\tilde{B}^1\Delta$								
cc-pVQZ EOM-CCSD	-100.298394	1.1625	1.3976	0.941	2915	909 <i>i</i>	1210	168.8(7.32)
cc-pVQZ EOM-CC3	-100.323321	1.1657	1.4276		2880	954 <i>i</i>	1072	164.4(7.13)
HBO $\tilde{a}^3\Sigma^+$								
cc-pVQZ EOM-CCSD	-100.342747	1.1642	1.3767	0.468	2888	900 <i>i</i>	1300	141.0(6.11)
cc-pVQZ EOM-CC3	-100.360915	1.1674	1.3937		2857	907 <i>i</i>	1208	140.8(6.11)
6-311+G(<i>d, p</i>) QCISD ^a		1.1682	1.3945					145.0(6.29) ^b
cc-pVTZ MRBWPT2 ^c		1.1495	1.3885					144.0(6.25)
HBO $\tilde{b}^3\Delta$								
cc-pVQZ EOM-CCSD	-100.319317	1.1624	1.3841	0.671	2913	974 <i>i</i>	1267	155.7(6.75)
cc-pVQZ EOM-CC3	-100.340569	1.1658	1.4055		2877	993 <i>i</i>	1160	153.6(6.66)
cc-pVTZ MR-BWPT2 ^c		1.1564	1.4046					155.2(6.73)

^aReference 31.

^bRelative energies from Ref. 31 are obtained with 6-311+G(*d, p*) QCISD(T) single points at the 6-311+G(*d, p*) QCISD optimized geometry.

^cReference 38.

TABLE V. Total energies and physical properties for linear BOH excited electronic states. [Energies are in hartrees, bond distances in angstrom, dipole moments in debye, harmonic vibrational frequencies in cm^{-1} , and energy differences in kcal mol^{-1} (eV).] Note that the $\tilde{a}^3\Sigma^+$ BOH excited electronic state dissociates to a BO $X^2\Sigma^+$ radical plus a 2S H atom, and is not presented in the Table.

Level of theory	Energy	$r_e(\text{B-O})$	$r_e(\text{O-H})$	μ_e^a	$\omega_1(\sigma)$	$\omega_2(\pi)$	$\omega_3(\sigma)$	ΔE^b
BOH $\tilde{A}^1\Sigma^+$								
cc-pVQZ EOM-CCSD	-100.301881	1.1896	1.4151	1.465	2360	523 <i>i</i>	1820	123.3 (5.35)
cc-pVQZ EOM-CC3	-100.337488	1.2002	1.4451		2684	480 <i>i</i>	1802	110.3 (4.78)
BOH $\tilde{B}^1\Pi$								
cc-pVQZ EOM-CCSD	-100.257256	1.2893	0.9419	2.787	4143	1324 <i>i</i> (647 <i>i</i>) ^c	1484	151.3 (6.56)
cc-pVQZ EOM-CC3	-100.274430	1.2948	0.9453		4089	1443 <i>i</i> (640 <i>i</i>)	1459	149.8 (6.50)
BOH $\tilde{b}^3\Pi$								
cc-pVQZ CCSD	-100.356655	1.3098	0.9388	2.077	4195	1121 <i>i</i> (528 <i>i</i>)	1451	88.9 (3.85)
cc-pVQZ CC3	-100.369583	1.3142	0.9417		4149	1122 <i>i</i> (523 <i>i</i>)	1430	90.1(3.91)
6-311+G(<i>d,p</i>) QCISD ^d		1.3214	0.9454					90.1 (3.91) ^e
cc-pVTZ MRBWP2 ^f		1.3009/ 1.3079	0.9428/ 0.9369					76.7 (3.33)/ 73.3 (3.18)

^aThe dipole direction of the $\tilde{A}^1\Sigma^+$ state is $^+\text{BOH}^-$, whereas the dipole direction of the $\tilde{B}^1\Pi$ and $\tilde{b}^3\Pi$ states is $^-\text{BOH}^+$.

^bEnergy differences are relative to the optimized \tilde{X}^1A' BOH structure.

^cDue to the Renner-Teller splitting, the a' and a'' components of the $\omega_2(\pi)$ harmonic vibrational frequency are nondegenerate. The a'' component is listed in parentheses.

^dReference 31.

^eRelative energies from Ref. 31 are obtained with 6-311+G(*d,p*) QCISD(T) single points at the 6-311+G(*d,p*) QCISD optimized geometry.

^fReference 38.

The EOM-CCSD dipole moment of the $\tilde{A}^1\Sigma^-$ state is 0.84 D, while the dipole moment of the $\tilde{B}^1\Delta$ state is 0.94 D. Charge localization on the boron atom (compared to the $\tilde{X}^1\Sigma^+$ ground state) reduces the magnitude of the $\tilde{A}^1\Sigma^-$ and $\tilde{B}^1\Delta$ dipole moments by a factor of three but retains the $^+\text{HBO}^-$ dipole direction. As the HB bond distance for these two states is in a range similar to the ground state, the EOM-CC3 HB stretching (ω_1) frequency has a similar value; 2882 cm^{-1} for the $\tilde{A}^1\Sigma^-$ state and 2880 cm^{-1} for the $\tilde{B}^1\Delta$ state. Inclusion of triple excitations with the EOM-CC3 wave function reduces the value of $\omega_3(\sigma)$ by more than 100 cm^{-1} compared to the EOM-CCSD method, with $\omega_3(\sigma) = 1095 \text{ cm}^{-1}$ for $\tilde{A}^1\Sigma^-$ and 1072 cm^{-1} for $\tilde{B}^1\Delta$. This trend generally continues among the investigated linear triplet excited states of HBO, as the triple excitations are crucial in properly describing the weak BO π bonding. Both excited electronic states have imaginary bending frequencies, 974*i* and 954*i* cm^{-1} , indicating respective bent equilibrium geometries.

E. Linear BOH singlet excited states

Energies, geometries, and physical properties of BOH linear excited states are presented in Table V. Preliminary computations of higher-lying $^1\Delta$ and $^1\Sigma^-$ BOH states, along with conclusions from the study of the BOH⁺ cation,³² imply that the BOH $\pi \rightarrow \pi^*$ excitation is unfavorable and leads to

some dissociated excited electronic states. The $\tilde{A}^1\Sigma^+$ BOH state comes from the 5σ nonbonding B atom lone pair being excited to the 6σ weakly OH antibonding MO, which tightens the BO bonding [$r_e(\text{BO})=1.2002 \text{ \AA}$] and creates a weaker OH bond [$r_e(\text{OH})=1.4451 \text{ \AA}$]. The EOM-CCSD method performs less well for this excited state, with geometries differing from EOM-CC3 by 0.01–0.03 Å . The highly ionic $\tilde{A}^1\Sigma^+$ excited state contains significant contribution from both single and double $5\sigma \rightarrow 6\sigma$ substitutions to the reference wave function, and EOM-CCSD fails to adequately describe this multireference character.

The dipole moment of the $\tilde{A}^1\Sigma^+$ state of BOH is predicted to be 1.47 D at the EOM-CCSD level of theory. Unlike other BOH excited states, the $\tilde{A}^1\Sigma^+$ BOH state has a dipole moment direction of $^+\text{BOH}^-$. Single and double $5\sigma \rightarrow 6\sigma$ excitations appear to shift enough charge density to change the direction of the dipole moment. The EOM-CC3 method yields an imaginary bending $\omega_2(\pi)$ frequency of 480*i* cm^{-1} , which implies a bent equilibrium geometry.

The $\tilde{B}^1\Pi$ state of BOH mainly involves single excitations from the reference coupled-cluster wave function, and thus EOM-CCSD and EOM-CC3 geometries agree more closely. The geometry and two harmonic vibrational stretching frequencies of the $\tilde{B}^1\Pi$ state are very similar to those of the BOH $\tilde{X}^1\Sigma^+$ ground state. While still large, the EOM-CCSD dipole moment of 2.79 D is smaller in magnitude

than that of the BOH $\tilde{X}^1\Sigma^+$ ground state. The $5\sigma \rightarrow 2\pi$ excitation shifts the charge density from the nonbonding B-atom lone pair to the π -antibonding MOs centered on the boron and oxygen atoms. Therefore, the negative charge remains localized on the B and O atoms, and the dipole direction is the same as that for the $\tilde{X}^1\Sigma^+$ state, namely $^-\text{BOH}^+$. The harmonic bending vibrational frequencies for this state show a case (d) Renner–Teller splitting.⁵⁹ The a' mode $\omega_2(\pi)$ has an imaginary frequency of $1443i \text{ cm}^{-1}$ and the a'' mode has an imaginary frequency of $640i \text{ cm}^{-1}$. Both the $^1A'$ and $^1A''$ components resulting from the linear $\tilde{B}^1\Pi$ state should have nonlinear equilibrium geometries with the $^1A'$ stationary point being lower in energy.

F. Linear HBO triplet excited states

Geometric parameters of the two HBO linear triplet excited states are shown in Table IV. Since $1\pi \rightarrow 2\pi$ excitation enhances BO antibonding and extends $r_e(\text{BO})$ by approximately 0.2 \AA , the geometries of the two linear triplet HBO excited states resemble their singlet counterparts with the same electron configuration. The dipole moments of these two states point in the same direction as the corresponding HBO singlet states, but with smaller magnitudes. The $\tilde{a}^3\Sigma^+$ and $\tilde{b}^3\Delta$ harmonic vibrational stretching frequencies are similar, both with respect to each other and to the isoconfigurational linear $\tilde{A}^1\Sigma^-$ and $\tilde{B}^1\Delta$ states of HBO. At the EOM-CC3 level of theory, both linear triplet states have imaginary $\omega_2(\pi)$ harmonic frequencies. The $\tilde{a}^3\Sigma^+$ $\omega_2(\pi)$ bending frequency is $907i \text{ cm}^{-1}$ and the $\tilde{b}^3\Delta$ value of $\omega_2(\pi)$ is $993i \text{ cm}^{-1}$, indicating bent equilibrium geometries for both states.

G. Linear BOH triplet excited states

Since the BOH $\tilde{A}^1\Sigma^+$ electronic state arising from the $\sigma \rightarrow \sigma^*$ excitation is lower lying than the $\tilde{B}^1\Pi$ state, it is expected that the triplet state arising from the $\sigma \rightarrow \sigma^*$ HOMO-LUMO excitation will be the lowest-lying excited electronic state of BOH. This excited electronic state does exist; however, it dissociates at all levels of theory to the same asymptote (BO $X^2\Sigma^+$ radical^{60,61} + 2S H atom) as the BOH ground state. Its bent counterpart, the \tilde{a}^3A' BOH electronic state, also dissociates to the BO $X^2\Sigma^+$ radical + 2S H atom. Contrary to the proposed state ordering of Gole and Michels,³¹ a consideration of this unbound (dissociative) excited electronic state allows us to label the first bound, linear triplet excited state of BOH as $\tilde{b}^3\Pi$, arising from the $5\sigma \rightarrow 2\pi$ excitation.

Geometries, dipole moments, and vibrational harmonic frequencies for the $\tilde{b}^3\Pi$ state are presented in Table V. This electronic state is well described by a single-reference coupled-cluster wave function, and higher accuracy is expected with the CC3 method compared to previous studies. Much like the $\tilde{B}^1\Pi$ state, the $\tilde{b}^3\Pi$ state qualitatively resembles the BOH ground state with a slightly extended $r_e(\text{BO})$ of 1.3142 \AA and an $r_e(\text{OH})$ of 0.9417 \AA . Contrary to the discussion of Peng *et al.*,³⁸ the first two bent triplet states

of BOH connect to the same linear BOH $\tilde{b}^3\Pi$ state. The linear $^3B_1/{}^3B_2$ components of this $^3\Pi$ state should give identical total energies and geometries when the BOH bond angle is constrained to 180° . We suspect that the use of two different active spaces to describe the \tilde{b}^3A' and \tilde{c}^3A'' electronic states by Peng *et al.* leads to a qualitatively incorrect PES near BOH linearity, providing nondegenerate total energies.

The dipole moment of the $\tilde{b}^3\Pi$ state has the same sign as the BOH ground state with a value of 2.08 D . Harmonic vibrational frequencies for the BOH $\tilde{b}^3\Pi$ state are similar to those of the BOH $\tilde{B}^1\Pi$ state. Bending frequencies are both imaginary and again show class (d) Renner–Teller splitting, with the a' $\omega_2(\pi)$ component having the larger imaginary frequency. The CC3 frequencies are a' $\omega_2(\pi) = 1122i \text{ cm}^{-1}$ and a'' $\omega_2(\pi) = 523i \text{ cm}^{-1}$. The two bent electronic states should be minima, with the $^3A'$ stationary point being lower in energy than the $^3A''$ state, akin to the BOH $\tilde{B}^1\Pi$ electronic state.

It has been shown that spin contamination affects the quality of open-shell UHF coupled-cluster wave functions⁶² and that the situation can be exacerbated when investigating open-shell excited states.⁶³ Szalay and Gauss surveyed a number of systems and found that “well-behaved” reference coupled-cluster wave functions led to nearly uncontaminated $\langle \hat{S}^2 \rangle$ values for excited states.⁶³ However, to our knowledge the expected lessening of spin contamination with UHF EOM-CC3 (vis-à-vis UHF EOM-CCSD) has not yet been examined. In this investigation, almost all EOM-CC3 triplet excited state wave functions are computed using the closed-shell ground state as a “false-UHF” reference. Therefore the triplet states characterized with this method are exactly spin-adapted and should present no spin contamination. The exceptions to this are the $\tilde{b}^3\Pi$ BOH electronic state and the corresponding bent \tilde{b}^3A' and \tilde{c}^3A'' BOH excited states. For these excited states, our reference $\langle \hat{S}^2 \rangle$ values for the UHF HBO/BOH linear and bent triplet states are never greater than 2.01 , close to the optimal $S(S+1)$ value of 2.00 . Therefore, spin contamination does not appear to be a concern in this study.

H. Bent HBO excited states

Optimized geometries and harmonic vibrational frequencies for the four bent HBO excited electronic states (\tilde{a}^3A' , \tilde{b}^3A'' , \tilde{A}^1A'' , and \tilde{B}^1A') are reported in Table VI. The geometries of the investigated singlet and triplet HBO bent excited states are similar, since they arise from the bending of isoconfigurational excited electronic states. The EOM-CC3 $r_e(\text{HB})$ of all four states ranges from 1.202 – 1.217 \AA , which represents a slight elongation from the associated linear states. The \tilde{a}^3A' state is predicted to have the shortest BO bond, $r_e = 1.356 \text{ \AA}$, which is also the case for the corresponding HBO $\tilde{a}^3\Sigma^+$ linear structure. Akin to the linear singlet and triplet excited electronic state structures, the EOM-CC3 $r_e(\text{BO})$ values for the bent excited states are 0.012 – 0.030 \AA

TABLE VI. Total energies and physical properties of bent HBO excited electronic states. [Energies are in hartrees, bond distances in angstrom, bond angles in degrees, harmonic vibrational frequencies in cm^{-1} , and relative energies in kcal mol^{-1} (eV, in parentheses) relative to the linear $\tilde{X}^1\Sigma^+$ HBO ground state.]

	Energy	$r_e(\text{H-B})$	$r_e(\text{B-O})$	$\angle\text{HBO}$	$\omega_1(a')$	$\omega_2(a')$	$\omega_3(a')$	ΔE
HBO \tilde{A}^1A''								
cc-pVQZ EOM-CCSD	-100.336308	1.1999	1.3864	125.33	2555	991	1274	145.0(6.29)
cc-pVQZ EOM-CC3	-100.364432	1.2043	1.4160	123.15				138.6(6.01)
HBO \tilde{B}^1A'								
cc-pVQZ EOM-CCSD	-100.314316	1.1993	1.3818	130.92	2541	840	1290	158.8(6.89)
cc-pVQZ EOM-CC3	-100.344300	1.2063	1.4111	126.75				151.3(6.56)
HBO \tilde{a}^3A'								
cc-pVQZ EOM-CCSD	-100.383485	1.2110	1.3439	109.82	2439	754	1352	115.4(5.00)
cc-pVQZ EOM-CC3	-100.402666	1.2171	1.3556	108.79				114.6(4.97)
6-311+G(d,p) QCISD ^a		1.2129	1.3609	110.94	2457	769	1306	113.9(4.94) ^b
cc-pVTZ MRBWP2 ^c		1.2124	1.3475	109.1				110.7(4.80)
HBO \tilde{b}^3A''								
cc-pVQZ EOM-CCSD	-100.350892	1.1977	1.3838	124.83	2580	982	1273	135.8(5.89)
cc-pVQZ EOM-CC3	-100.375607	1.2019	1.4100	122.94				131.6(5.71)
cc-pVTZ MRBWP2 ^c		1.1797	1.3914	120.1				125.9(5.46)

^aReference 31.

^bRelative energies from Ref. 31 were obtained with the 6-311+G(d,p) QCISD(T)//QCISD 6-311+G(d,p) level of theory.

^cReference 38.

longer than those obtained with EOM-CCSD. With a tighter BO bond and a weaker HB bond, the \tilde{a}^3A' state has the smallest $\angle\text{HBO}$ of 108.8° .

All harmonic vibrational frequencies for the \tilde{a}^3A' , \tilde{b}^3A'' , \tilde{A}^1A'' , and \tilde{B}^1A' excited states are real, validating these bent structures as minima, and most harmonic vibrational frequencies resemble the values of their linear counterparts. As the $\tilde{B}^1\Delta$ state is higher in energy and possesses a smaller imaginary $\omega_2(\pi)$ frequency than the $\tilde{A}^1\Sigma^-$ state, the HBO \tilde{A}^1A'' state is formed from the $^1A''$ resolution of the $\tilde{A}^1\Sigma^-$ state and the \tilde{B}^1A' state from the $^1A'$ component of the $\tilde{B}^1\Delta$ state. The \tilde{a}^3A' state arises from the $^3A'$ resolution of the $\tilde{a}^3\Sigma^+$ state, and the \tilde{b}^3A'' state from the $^3A''$ component of the $\tilde{b}^3\Delta$ state.

I. Bent BOH excited states

The equilibrium geometries and harmonic vibrational frequencies for the characterized bent BOH excited electronic states (\tilde{b}^3A' , \tilde{c}^3A'' , \tilde{A}^1A' , \tilde{B}^1A' , and \tilde{C}^1A'') are presented in Table VII. The \tilde{A}^1A' state has different geometric parameters from the other characterized BOH excited states, with an EOM-CC3 $r_e(\text{BO})$ of 1.243 \AA and an $r_e(\text{OH})$ of 1.571 \AA , suggesting a very loose OH bond. The inclusion of partial triple excitations into the EOM-CC wave function affects the geometry and relative energy of the BOH \tilde{A}^1A' state, more so than other excited electronic states of HBO and BOH. As will be discussed below, the ground state BOH total energy rises sharply upon $r_e(\text{OH})$ elongation, and it is expected that at the \tilde{A}^1A' optimized geometry the ground state wave function contains multireference character as

well, justifying the benefits of the EOM-CC3 method. An analysis of the MOs and the similarities between the BOH $\tilde{A}^1\Sigma^+$ and \tilde{A}^1A' bond distances provide a convincing argument that the \tilde{A}^1A' state is derived from the $^1A'$ resolution of the $\tilde{A}^1\Sigma^+$ state, rather than the $^1A'$ component of the $\tilde{B}^1\Pi$ state.

As noted, upon bending of either the BOH $\tilde{B}^1\Pi$ state or the $\tilde{b}^3\Pi$ state, Renner–Teller splitting necessarily forms non-degenerate electronic states. Since the $\omega_2(\pi)$ a' component of the BOH $\tilde{B}^1\Pi$ state has a larger imaginary frequency than the a'' component, the \tilde{B}^1A' state connected to the $\tilde{B}^1\Pi$ state lies energetically between the bent \tilde{A}^1A' state and the \tilde{C}^1A'' state. The bond lengths and harmonic vibrational frequencies of all investigated BOH bent excited electronic states generally resemble their linear counterparts. The \tilde{b}^3A' , \tilde{c}^3A'' , \tilde{A}^1A' , \tilde{B}^1A' , and \tilde{C}^1A'' excited electronic states of BOH each have three real harmonic vibrational frequencies, and thus each is a genuine minimum.

Figure 1 schematically depicts adiabatic transition energies relative to the linear HBO $\tilde{X}^1\Sigma^+$ ground state, and all investigated excited electronic states show bent minima and a likely isomerization transition state (to BOH) at a $\angle\text{BOH}$ of 40° – 80° . The same qualitative “double-well” phenomenon as that of Gole and Michels³¹ and of Peng *et al.*³⁸ is observed for the PES of the two lowest-lying triplet states. The electronic structure of the system changes dramatically in the region of the isomerization transition states, from preferential HBO $\pi \rightarrow \pi^*$ character to BOH $\sigma \rightarrow \pi^*$ or $\sigma \rightarrow \sigma^*$ character. As a consequence, the excited state isomerization PESs could connect different linear electronic states.

TABLE VII. Total energies and physical properties of bent BOH excited electronic states. [Energies are in hartrees, bond distance in angstrom, bond angles in degrees, harmonic vibrational frequencies in cm^{-1} , and adiabatic transition energies in kcal mol^{-1} (eV, in parentheses) relative to the bent \tilde{X}^1A' BOH ground state.] Note that the \tilde{a}^3A' excited state dissociates to a BO $X^2\Sigma^+$ radical plus a 2S H atom and is not presented in the table.

	Energy	$r_e(\text{B-O})$	$r_e(\text{O-H})$	$\angle\text{BOH}$	$\omega_1(a')$	$\omega_2(a')$	$\omega_3(a')$	ΔE
BOH \tilde{A}^1A'								
cc-pVQZ EOM-CCSD	-100.316612	1.2278	1.5311	115.18	2156	558	1498	114.0(4.94)
cc-pVQZ EOM-CC3	-100.350887	1.2425	1.5712	114.69				101.9(4.42)
BOH \tilde{B}^1A'								
cc-pVQZ EOM-CCSD	-100.293121	1.3455	0.9690	113.71	3475	989	1308	128.8(5.58)
cc-pVQZ EOM-CC3	-100.310081	1.3490	0.9766	114.16				127.5(5.53)
BOH \tilde{C}^1A''								
cc-pVQZ EOM-CCSD	-100.271645	1.3739	0.9616	112.01	3866	825	1155	142.2(6.17)
cc-pVQZ EOM-CC3	-100.288666	1.3811	0.9657	111.45				140.9(6.11)
BOH \tilde{b}^3A'								
cc-pVQZ CCSD	-100.388092	1.3402	0.9603	113.98	3792	1081	1363	69.2(3.00)
cc-pVQZ CC3	-100.401354	1.3457	0.9641	113.55	3730	1064	1338	70.2(3.04)
6-311+G(<i>d,p</i>) QCISD ^a		1.3506	0.9640	112.49	3794	1094	1328	68.8(2.99)
cc-pVTZ MR-BWPT2 ^c		1.3409	0.9641	113.05				58.2(2.52)
BOH \tilde{c}^3A''								
cc-pVQZ CCSD	-100.364030	1.3585	0.9530	120.10	3982	699	1298	84.3(3.65)
cc-pVQZ CC3	-100.376887	1.3633	0.9563	119.76	3935	686	1278	85.5(3.71)
cc-pVTZ MR-BWPT2 ^c		1.3406	0.9514	125.38				70.4(3.05)

^aReference 31.

^bRelative energies from Ref. 31 were obtained with the 6-311+G(*d,p*) QCISD(T) // QCISD 6-311+G(*d,p*) level of theory.

^cReference 38.

J. Adiabatic and vertical transition energies of excited states

The adiabatic transition energies of the stationary points are displayed in the last column of Tables III–VII and pictorially in Fig. 1. For HBO, the energetic EOM-CC3 T_e ordering for minima found in this research is in kcal mol^{-1} ,

$$0(\tilde{X}^1\Sigma^+) < 115(\tilde{a}^3A') < 132(\tilde{b}^3A'') < 139(\tilde{A}^1A'') < 151(\tilde{B}^1A'),$$

and the BOH energetic ranking is

$$0(\tilde{X}^1A') < 70(\tilde{b}^3A') < 86(\tilde{c}^3A'') < 102(\tilde{A}^1A'') < 128(\tilde{B}^1A') < 141(\tilde{C}^1A'').$$

As expected, the smaller and highly geometry-dependent HOMO-LUMO gap of \tilde{X}^1A' BOH brings about a denser cluster of BOH excited electronic states. Our adiabatic energies are in excellent agreement for those of the \tilde{b}^3A' electronic state investigated by Gole and Michels.³¹ However, while our HBO T_e values agree with those of the Peng *et al.* study,³⁸ our BOH adiabatic transition energies are often 13–15 kcal mol^{-1} larger. We suspect that their use of different active spaces for the $^3A'$ and $^3A''$ states may create an artificial lowering of the $^3A''$ PES total energy. It is also possible that the MR-BWPT2 method does not recover enough dynamical correlation in the near-equilibrium region of the BOH \tilde{X}^1A' ground state.

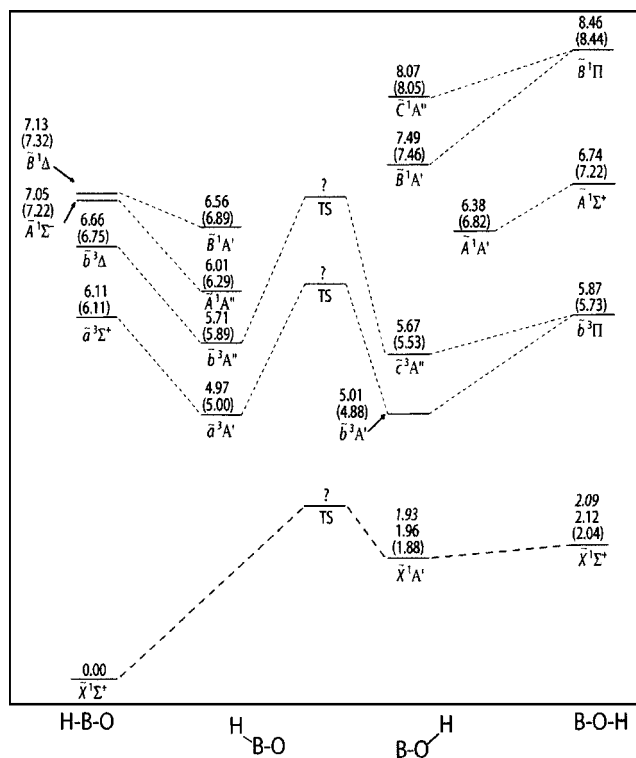


FIG. 1. Schematic of the HBO and BOH ground and excited electronic state transition energies (in eV). Adiabatic transition energies at the cc-pVQZ CC3/EOM-CC3 level of theory are reported relative to the CC3 $\tilde{X}^1\Sigma^+$ HBO minimum. Isomeric CCSDT ground-state energies are reported in italics relative to the CCSDT $\tilde{X}^1\Sigma^+$ HBO global minimum. In parentheses, CCSD/EOM-CCSD adiabatic energies are reported relative to the CCSD $\tilde{X}^1\Sigma^+$ HBO minimum. As indicated by the question marks, the positions of the transition states are less well known, but sketched here from the work of Refs. 31 and 38.

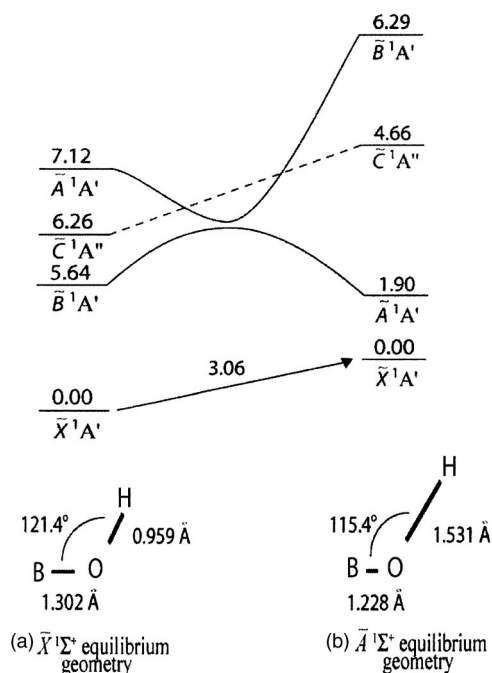


FIG. 2. Vertical excitation energies at the cc-pVQZ CCSD/EOM-CCSD level of theory of singlet BOH excited states (in eV) at (a) the equilibrium geometry of the \tilde{X}^1A' BOH ground electronic state and (b) the equilibrium geometry of the \tilde{A}^1A' BOH excited electronic state. The arrow connecting the two columns shows the difference of the \tilde{X}^1A' ground-state energy (a) at its equilibrium geometry and (b) at the \tilde{A}^1A' equilibrium geometry with an elongated OH bond.

The CC3 $\tilde{b}^3A' \leftarrow \tilde{X}^1A'$ adiabatic T_e for BOH is 3.04 eV, in agreement with the theoretical prediction of 2.99 eV by Gole and Michels,³¹ while the CC3 BOH $\tilde{c}^3A'' \leftarrow \tilde{X}^1A'$ adiabatic excitation energy is 3.71 eV. The vertical $\tilde{b}^3A' \leftarrow \tilde{X}^1A'$ transition energy is 3.10 eV with the CC3 method, and the $\tilde{c}^3A'' \leftarrow \tilde{X}^1A'$ vertical excitation energy is 3.81 eV, which is much larger than the prediction of ~ 3.05 eV by Peng *et al.*³⁸

Because of the large geometric elongation of the OH bond length at the BOH \tilde{A}^1A' excited state minimum (compared to that of the \tilde{X}^1A' BOH ground state), the singlet vertical excitation energies require careful analysis and are represented pictorially in Fig. 2. In the PES region of the \tilde{A}^1A' geometric equilibrium (with the OH bond significantly elongated), the ground state is much higher in energy, with an EOM-CCSD $\tilde{X}^1A'/\tilde{A}^1A'$ excitation energy of only 1.90 eV. Note that the ground-state energy required for such an $r(\text{OH})$ elongation is approximately 3.06 eV. Figure 2 indicates that the BOH ground state, the \tilde{B}^1A' state, and the \tilde{C}^1A'' state all travel significantly “uphill” along the stretched OH bond coordinate.

The BOH \tilde{X}^1A' equilibrium geometry resembles the geometries of the \tilde{B}^1A' and \tilde{C}^1A'' excited electronic states more than that of the \tilde{A}^1A' electronic state. Hence, the \tilde{B}^1A' state has a lower EOM-CCSD vertical excitation energy (5.64 eV) than the \tilde{A}^1A' state (7.12 eV). Due to the large shift in relative state energies along the potential-energy

curve for $r_e(\text{OH})$ stretching, both conical intersections^{64–66} and avoided crossings occur. Along this stretching coordinate, there will be $\tilde{A}^1A'/\tilde{C}^1A''$ and $\tilde{B}^1A'/\tilde{C}^1A''$ conical intersections, as well as an $\tilde{A}^1A'/\tilde{B}^1A'$ avoided crossing. The mapping of PESs and such conical intersections may lend well to theoretical elaboration, but is outside the scope of this investigation.

Gole and Michels infer that for excitation intensity borrowing to be possible, the energy difference between the first excited singlet and lowest triplet BOH states at the \tilde{X}^1A' BOH equilibrium geometry should be similar to the isoelectronic $A^1\Pi/a^3\Pi$ boron monofluoride vertical excitation energy difference of 2.73 eV.³¹ The computed CC3/EOM-CC3 vertical energy difference between the $\tilde{b}^3A' \leftarrow \tilde{X}^1A'/\tilde{B}^1A' \leftarrow \tilde{X}^1A'$ electronic transitions is 2.78 eV. Our agreement with previous theoretical work and empirical observation sustains the possibility of singlet-triplet excited state intensity borrowing.

To function as a HEDM material, electronic excitation to a vibrationally excited triplet BOH state will be necessary to allow possible isomerization via the TS barriers in Fig. 1. However, dissociative HBO electronic states arising from the $\pi \rightarrow \sigma^*$ excitation and unbound BOH electronic states from the $\pi \rightarrow \pi^*$ or $\pi \rightarrow \pi^*$ excitations may lie near the excitation energy of the highly vibrationally excited low-lying triplet states. Quanta absorbed into BOH stretching modes may break apart the molecule if the bent \tilde{b}^3A' and \tilde{c}^3A'' PESs approach dissociative pathways.

V. CONCLUSIONS

The $\tilde{X}^1\Sigma^+$ HBO ground-state global minimum, the \tilde{X}^1A' BOH ground state, and the linear $\tilde{X}^1\Sigma^+$ BOH transition state have been studied using *ab initio* methods with the cc-pVQZ basis sets. Stationary points for the HBO $\tilde{A}^1\Sigma^-$, $\tilde{B}^1\Delta$, $\tilde{a}^3\Sigma^+$, and $\tilde{b}^3\Delta$ excited states as well as the BOH $\tilde{A}^1\Sigma^+$, $\tilde{B}^1\Pi$, and $\tilde{b}^3\Pi$ excited states and their bent counterparts have been characterized with a new implementation of excited state coupled-cluster theory (CC3). The harmonic vibrational frequency analyses of the linear and bent excited states indicate that all excited electronic states characterized here have bent minima.

This study provides the first consistent set of predictions for the singlet excited electronic states of HBO and BOH. The energy ordering of the bound minima are $\tilde{X}^1\Sigma^+ < \tilde{a}^3A' < \tilde{b}^3A' < \tilde{A}^1A'' < \tilde{B}^1A'$ for HBO and $\tilde{X}^1A' < \tilde{b}^3A' < \tilde{c}^3A'' < \tilde{A}^1A' < \tilde{B}^1A' < \tilde{C}^1A''$ for BOH. The \tilde{a}^3A' HBO and \tilde{b}^3A' BOH states are both ~ 115 kcal mol⁻¹ (5.0 eV) higher in energy than $\tilde{X}^1\Sigma^+$ HBO. The lowest excited singlet states are \tilde{A}^1A'' for HBO, with a predicted T_e of 139 kcal mol⁻¹ (6.01 eV) and \tilde{A}^1A' for BOH, with a T_e value of 148 kcal mol⁻¹ (6.40 eV). The HBO $\pi \rightarrow \pi^*$ excitation from the ground electronic state causes a lengthening of the BO bond and a lessening of the dipole moment magnitude, while the BOH $\sigma \rightarrow \sigma^*$ excitation severely lengthens

the OH bond and causes a change in the direction of the dipole moment. On the other hand, the BOH $\sigma \rightarrow \pi^*$ excitation slightly elongates the BO bond and decreases the dipole moment.

The EOM-CC3 method is found to be more accurate than the EOM-CCSD method, especially for the two BOH excited states (\tilde{a}^3A' and \tilde{A}^1A') arising from the $\sigma \rightarrow \sigma^*$ excitation. The EOM-CC methods provide both closed- and open-shell excited electronic state total energies, geometric properties, and harmonic vibrational frequencies in a nearly "black box" manner. Singlet-triplet vertical and adiabatic transition energies are predicted at an accuracy that exceeds previous theoretical studies. Assuming the challenge of synthesizing and storing BOH in sufficient amounts is met, traversing the excited state isomerization PES of BOH to HBO may be treacherous due to dissociative excited electronic states along the proposed reaction pathway. Obviously, much more theoretical and experimental work must be carried out to test the viability of BOH as a high-energy density material.

ACKNOWLEDGMENTS

We would like to thank Dr. Kurt W. Sattelmeyer for his patience as well as his invaluable assistance with ACES II. Professor Wesley D. Allen is thanked for frequent discussions and advice. This research was performed in part using the Molecular Science Computing Facility (MSCF) in the William R. Wiley Environmental Molecular Sciences Laboratory, a national scientific user facility sponsored by the U.S. Department of Energy's Office of Biological and Environmental Research and located at the Pacific Northwest National Laboratory (PNL). PNL is operated for the Department of Energy by Battelle. This research was supported by the U.S. Department of Energy, under the Chemical Physics Program.

¹M. Page, *J. Phys. Chem.* **93**, 3639 (1989).

²J. A. Harrison and R. G. A. R. Maclagan, *Chem. Phys. Lett.* **155**, 419 (1989).

³L. Andrews and T. R. Burkholder, *J. Phys. Chem.* **95**, 8554 (1991).

⁴C.-H. Chin, A. M. Mebel, and D. Y. Hwang, *J. Phys. Chem. A* **108**, 473 (2004).

⁵G. W. Burdette, H. R. Lander, and J. R. McCoy, *J. Energy* **2**, 289 (1978).

⁶R. C. Brown, C. E. Kolb, S. Y. Cho, R. A. Yetter, F. L. Dryer, and H. Rabitz, *Int. J. Chem. Kinet.* **26**, 319 (1994).

⁷M. K. King, in *Combustion of Boron-Based Solid Propellants and Solid Fuels*, edited by K. K. Kuo and R. Pein (Begell House, New York, 1993), p. 1.

⁸A. Ulas, K. K. Kuo, and C. Gotzmer, *Combust. Flame* **127**, 1935 (2001).

⁹R. F. Porter and W. P. Sholette, *J. Chem. Phys.* **37**, 198 (1962).

¹⁰W. P. Sholette and R. F. Porter, *J. Phys. Chem.* **67**, 177 (1963).

¹¹L. Barton, F. A. Grimm, and R. F. Porter, *Inorg. Chem.* **5**, 2076 (1966).

¹²E. R. Lory and R. F. Porter, *J. Am. Chem. Soc.* **93**, 6301 (1971).

¹³C. Thomson and B. J. Wishart, *Theor. Chim. Acta* **35**, 267 (1974).

¹⁴R. S. Mulliken, *J. Chem. Phys.* **23**, 1833 (1955).

¹⁵N. L. Summers and J. Tyrrell, *J. Am. Chem. Soc.* **99**, 3960 (1977).

¹⁶T. S. Zyubina, O. P. Charkin, and L. V. Gurvich, *J. Struct. Chem.* **20**, 1 (1979).

¹⁷P. K. Pearson, H. F. Schaefer, and U. Wahlgren, *J. Chem. Phys.* **62**, 350 (1975).

¹⁸A. D. Walsh, *J. Chem. Soc.* **1953**, 2260.

¹⁹R. F. W. Bader, *Can. J. Chem.* **40**, 1164 (1962).

²⁰K. Fukui, *Acc. Chem. Res.* **4**, 57 (1971).

²¹H. F. Schaefer, *The Electronic Structure of Atoms and Molecules: A Sur-*

vey of Rigorous Quantum Mechanical Results (Addison-Wesley, Reading, MA, 1972).

²²R. J. Buenker and S. D. Peyerimhoff, *Chem. Rev. (Washington, D.C.)* **74**, 127 (1974).

²³B. M. Gimarc, *Molecular Structure and Bonding: The Qualitative Molecular Orbital Approach* (Academic, New York, 1979).

²⁴Y. Kawashima, K. Kawaguchi, and E. Hirota, *Chem. Phys. Lett.* **131**, 205 (1986).

²⁵Y. Kawashima, Y. Endo, K. Kawaguchi, and E. Hirota, *Chem. Phys. Lett.* **135**, 441 (1987).

²⁶Y. Kawashima, Y. Endo, and E. Hirota, *J. Mol. Spectrosc.* **133**, 116 (1989).

²⁷E. R. Talaty, Y. Huang, and M. E. Zandler, *J. Am. Chem. Soc.* **113**, 779 (1991).

²⁸M. T. Nguyen, P. J. Groarke, and T.-K. Ha, *Mol. Phys.* **75**, 1105 (1992).

²⁹T.-K. Ha and J. Makarewicz, *Chem. Phys. Lett.* **299**, 637 (1999).

³⁰C. A. Richards, G. Vacek, B. J. Deleeuw, Y. Yamaguchi, and H. F. Schaefer, *J. Chem. Phys.* **102**, 1280 (1995).

³¹J. L. Gole and H. H. Michels, *J. Chem. Phys.* **103**, 7844 (1995).

³²A. I. Boldyrev and J. Simons, *J. Chem. Phys.* **110**, 3765 (1999).

³³M. Sobczyk, I. Anusiewicz, P. Skurski, and J. Simons, *Mol. Phys.* **101**, 1259 (2003).

³⁴C. M. Tarver, *J. Phys. Chem. A* **101**, 4845 (1997).

³⁵M. R. Manaa and L. E. Fried, *J. Phys. Chem. A* **103**, 9349 (1999).

³⁶E. J. Reed, J. D. Joannopoulos, and L. E. Fried, *Phys. Rev. B* **62**, 16500 (2000).

³⁷L. E. Fried, M. R. Manaa, P. F. Pagoria, and R. L. Simpson, *Annu. Rev. Mater. Res.* **31**, 291 (2001).

³⁸Q. Peng, Y. B. Wang, B. Suo, Q. Z. Shi, and Z. Y. Wen, *J. Chem. Phys.* **121**, 778 (2004).

³⁹G. Herzberg, *Electronic Spectra and Electronic Structure of Polyatomic Molecules* (Van Nostrand Reinhold, New York, 1966).

⁴⁰Y. Yamaguchi, B. J. Deleeuw, G. Vacek, C. A. Richards, and H. F. Schaefer, *J. Chem. Phys.* **101**, 3006 (1994).

⁴¹See EPAPS Document No. E-JCPA6-123-315525 for the derivation of electron configurations of the possible HBO/BOH excited states. This document can be reached via a direct link in the online article's HTML reference section or via the EPAPS homepage (<http://www.aip.org/pubservs/epaps.html>).

⁴²R. J. Bartlett, in *Modern Electronic Structure Theory, Advanced Series in Physical Chemistry Vol. 2*, edited by D. R. Yarkony (World Scientific, Singapore, 1995), p. 1047.

⁴³T. D. Crawford and H. F. Schaefer, *Rev. Comput. Chem.* **14**, 33 (2000).

⁴⁴G. D. Purvis and R. J. Bartlett, *J. Chem. Phys.* **76**, 1910 (1982).

⁴⁵K. Raghavachari, G. W. Trucks, J. A. Pople, and M. Head-Gordon, *Chem. Phys. Lett.* **157**, 479 (1989).

⁴⁶T. J. Lee and G. E. Scuseria, in *Quantum Mechanical Electron Structure Calculations with Chemical Accuracy*, edited by S. R. Langhoff (Kluwer, Dordrecht, 1995), p. 47.

⁴⁷H. Koch, O. Christiansen, P. Jørgensen, A. M. S. deMeras, and T. Helgaker, *J. Chem. Phys.* **106**, 1808 (1997).

⁴⁸J. Noga and R. J. Bartlett, *J. Chem. Phys.* **86**, 7041 (1987).

⁴⁹J. D. Watts and R. J. Bartlett, *J. Chem. Phys.* **93**, 6104 (1990).

⁵⁰J. F. Stanton and R. J. Bartlett, *J. Chem. Phys.* **98**, 7029 (1993).

⁵¹J. F. Stanton and J. Gauss, *Theor. Chim. Acta* **91**, 267 (1995).

⁵²O. Christiansen, H. Koch, and P. Jørgensen, *J. Chem. Phys.* **103**, 7429 (1995).

⁵³T. H. Dunning, Jr., *J. Chem. Phys.* **90**, 1007 (1989).

⁵⁴D. E. Woon and T. H. Dunning Jr., *J. Chem. Phys.* **103**, 4572 (1995).

⁵⁵J. F. Stanton, J. Gauss, J. D. Watts, W. J. Lauderdale, and R. J. Bartlett, ACES II, an *ab initio* program system. This package also contains modified versions of the MOLECULE Gaussian integral program of J. Almof and P. R. Taylor, the ABACUS integral derivative program written by T. Helgaker, H. J. Aa. Jensen, P. Jørgensen, and P. R. Taylor, and the PROPS property integral code of P. R. Taylor.

⁵⁶T. D. Crawford, C. D. Sherrill, E. F. Valeev *et al.*, PSI 3.2 (2003).

⁵⁷J. F. Stanton, C. L. Lopreore, and J. Gauss, *J. Chem. Phys.* **108**, 7190 (1998).

- ⁵⁸Y. He, Z. He, and D. Cremer, *Theor. Chem. Acc.* **105**, 182 (2001).
- ⁵⁹T. J. Lee, D. J. Fox, H. F. Schaefer, and R. M. Pitzer, *J. Chem. Phys.* **81**, 356 (1984).
- ⁶⁰F. Melen, I. Dubois, and H. Bredohl, *J. Mol. Spectrosc.* **208**, 14 (2001).
- ⁶¹F. Melen, I. Dubois, and H. Bredohl, *J. Phys. B* **18**, 2423 (1985).
- ⁶²J. F. Stanton, *J. Chem. Phys.* **101**, 371 (1994).
- ⁶³P. G. Szalay and J. Gauss, *J. Chem. Phys.* **112**, 4027 (2000).
- ⁶⁴E. Teller, *J. Phys. Chem.* **41**, 109 (1937).
- ⁶⁵D. R. Yarkony, *Rev. Mod. Phys.* **68**, 985 (1996).
- ⁶⁶D. R. Yarkony, *J. Phys. Chem. A* **105**, 6277 (2001).